

g-wave Pairing in BiS₂ Superconductors

Xianxin Wu,¹ Jing Yuan,¹ Yi Liang,¹ Heng Fan,¹ and Jiangping Hu^{1,2,*}

¹ *Institute of Physics, Chinese Academy of Sciences, Beijing 100190, China*

² *Department of Physics, Purdue University, West Lafayette, Indiana 47907, USA*

(Dated: November 8, 2018)

Recent angle resolved photoemission spectroscopy (ARPES) experiments have suggested that BiS₂ based superconductors are at very low electron doping. Using random phase approximation (RPA) and functional renormalization group (FRG) methods, we find that *g*-wave pairing symmetry belonging to A_{2g} irreducible representation is dominant at electron doping $x < 0.25$. The pairing symmetry is determined by inter-pocket nesting and orbital characters on the Fermi surfaces and is robust in a two-orbital model including both Hund's coupling J , and Hubbard-like Coulomb interactions U and U' with relatively small J ($J \leq 0.2U$). With the increasing electron doping, the *g*-wave state competes with both the *s*-wave A_{1g} and *d*-wave B_{2g} states and no pairing symmetry emerges dominantly.

PACS numbers: 74.20.Mn, 74.20.Rp, 74.70.Dd

Recently, a new family of materials containing BiS₂ layers has been discovered to be superconducting (SC) and drawn many research attentions [1–11]. Similar to cuprate and iron based superconductors, these materials consist of two dimensional BiS₂ layers and various types of blocking layers. The essential electronic properties are attributed to the BiS₂ layers. According to density functional theory calculations, the parent compounds of the BiS₂-based superconductors are semiconducting and the conduction band is mainly attributed to the $6p$ orbitals of Bi [1, 12]. A two-orbital model, including Bi p_X and p_Y orbitals, reasonably describes the band structure [12] that controls major electronic properties. Superconductivity is induced by electron doping.

Due to the weak correlation effect in p orbitals and the low superconducting transition temperature, electron phonon coupling has been suggested to play a dominant role in superconducting pairing [13–15]. However, in the recent neutron scattering experiment, the observed almost unchanged low-energy modes indicated that the electron phonon coupling could be much weaker than expected [16]. Moreover, the large ratio $2\Delta/T_c$ may suggest that the pairing mechanism is unconventional [17, 18]. Electron-electron correlations can be responsible for the Copper pairing [19–22].

When electron-electron correlations are the driving force for pairing, unconventional pairing symmetries arise naturally. There have been quite a few theoretical studies about possible pairing symmetries in these new superconductors [19–22]. As the nominal compositions of the superconducting materials indicated high electron doping [3, 11], all these previous studies concentrated on the high electron doping region where the electronic structure was featured with large Fermi surfaces (FS) at Γ and M points in Broullion zone (BZ) in close vicinity to Van Hove singularity. However, very recently, two ARPES groups have reported that there are only two small electron pockets around X points [23, 24] and the true electron fillings are much smaller than those expected from the nominal compositions.

In this paper, we investigate the pairing symmetry of BiS₂ based superconductors at low doping level using ran-

dom phase approximation (RPA) and functional renormalization group (FRG) methods. We find that *g*-wave pairing state that belongs to the A_{2g} irreducible representations of the lattice symmetry is dominant at electron doping $x < 0.25$ in a two-orbital model including both Hund's coupling J , and Hubbard-like Coulomb interactions U and U' in the reasonable parameter region $J \leq 0.2U$. This robust pairing symmetry is determined by inter pocket nesting and orbital characters on the FS. With the increase of J or electron doping level, the *g*-wave loses its dominance and competes with other pairing symmetries. In both cases, there is no single dominant pairing wave. For example, with a large J , a *d*-wave (B_{1g}) is only slightly favored over a *s*-wave (A_{1g}) and the *g*-wave, and at high doping near the Lifshitz transition on which the previous studies concentrated, the *s*-wave and the other *d*-wave (B_{2g}) are almost equally favored. Due to the close competition between *s*-wave and *d*-wave, we speculate that superconductivity may not take place at high electron doping. Our results, therefore, predict a new pairing symmetry for the BiS₂ superconductors. As the *g*-wave pairing state has a distinct nodal structure on FS, our prediction can be experimentally tested.

We adopt the two-band model, the tight binding Hamiltonian [12] is $H_0 = \sum_{\mathbf{k}\sigma} \Psi_{\mathbf{k}\sigma}^\dagger T(\mathbf{k}) \Psi_{\mathbf{k}\sigma}$,

$$T(\mathbf{k}) = \begin{pmatrix} \epsilon_X(\mathbf{k}) - \mu & \epsilon_{XY}(\mathbf{k}) \\ \epsilon_{XY}(\mathbf{k})^* & \epsilon_Y(\mathbf{k}) - \mu \end{pmatrix} \quad (1)$$

where $\Psi_{\mathbf{k}\sigma}^\dagger = (c_{X\mathbf{k}\sigma}^\dagger, c_{Y\mathbf{k}\sigma}^\dagger)$ is the creation operator for spin σ electrons in the two orbitals p_X, p_Y and $\epsilon_X(\mathbf{k})$, $\epsilon_Y(\mathbf{k})$ and $\epsilon_{XY}(\mathbf{k})$ are the same as those defined in Ref. [20]. As the observed electron doping is much less than those inferred from the nominal composition, we discuss the pairing properties based on FS before the Lifshitz transition. For the case after Lifshitz transition, RPA calculations have been done in Ref. [21]. Fig. 1(a) shows the FS electron pockets for four different electron fillings $x = 0.08, 0.14, 0.25$ and 0.45 . The corresponding bare spin susceptibilities are shown in Fig. 1(b). There is a rectangle-shaped electron pocket centered at each X point for $x = 0.14$. Compared with experimental data [23, 24], a smaller electron pocket at X point is absent because the real

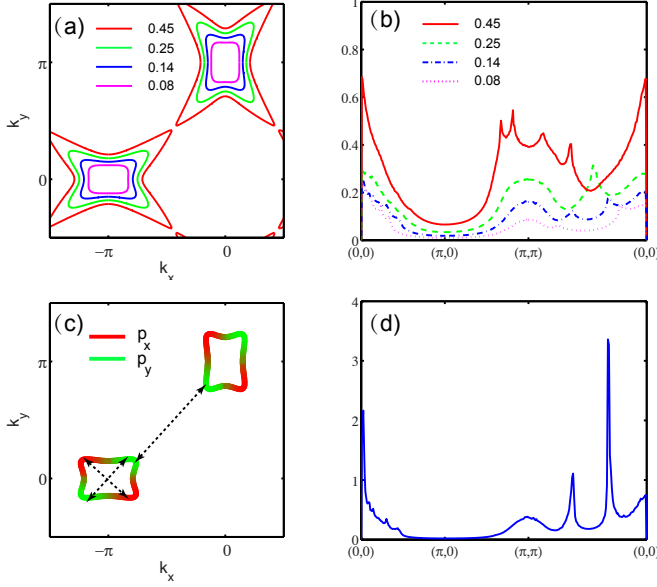


FIG. 1: (Color online) (a) Fermi surfaces for different electron doping. (b) The bare susceptibility for the same electron fillings as in (a). (c) The orbital characters on FS for $x=0.14$. The main contributions are shown by the following colors: red for p_x and green for p_y . The FS nesting vectors are indicated by black lines with arrows. (d) The RPA susceptibility for $x=0.14$ with $U=3.5$ and $J=0$. The positions of two sharp peaks on the right correspond to the nesting vectors shown in (c).

materials contain two BiS_2 layers but the model is based on a single BiS_2 layer and neglects the interlayer coupling. The orbital characters on FS are shown in Fig. 1(c), where the colors correspond to the dominant orbital weight (red for p_x and green for p_y). The two right peaks (in blue dash dot line) at $\mathbf{q}_1 = (0.62\pi, 0.62\pi)$ and $\mathbf{q}_2 = (0.32\pi, 0.32\pi)$ correspond to inter and intra FS nesting, respectively. The broad peak at (π, π) , interpreted as inter pocket nesting, resembles the FS nesting in iron based superconductors[25]. The nesting wave vectors are shown in Fig. 1(c). When interactions are introduced, the peaks at \mathbf{q}_1 and \mathbf{q}_2 in χ_0 are the ones that diverge in the RPA spin susceptibility (Fig. 1(d)). With the increasing of electron doping, \mathbf{q}_1 moves right but \mathbf{q}_2 moves left. Near the Lifshitz transition point ($x=0.45$), the broad peak disappears and many peaks appear in χ_0 due to the inter pocket FS nesting. The RPA spin susceptibility diverges at certain \mathbf{k} , indicating that the system is unstable to a long range magnetic order. At low doping concentration ($x < 0.2$), the FS are rectangle-shaped. The orbital characters on FS and inter pockets nesting clearly play a crucial role in determining the pairing symmetry.

The interaction part of Hamiltonian for this multi-orbital

system is,

$$H_{int} = U \sum_{i\alpha} n_{i\alpha\uparrow} n_{i\alpha\downarrow} + U' \sum_{i,\alpha<\beta} n_{i\alpha} n_{i\beta} + J \sum_{i,\alpha<\beta,\sigma\sigma'} c_{i\alpha\sigma}^\dagger c_{i\beta\sigma'}^\dagger c_{i\alpha\sigma'} c_{i\beta\sigma} + J' \sum_{i,\alpha\neq\beta} c_{i\alpha\uparrow}^\dagger c_{i\alpha\downarrow}^\dagger c_{i\beta\downarrow} c_{i\beta\uparrow} \quad (2)$$

where $n_{i\alpha} = n_{i\alpha\uparrow} + n_{i\alpha\downarrow}$. Here we adopt the parameter notations given in Ref.[26]. The effective interaction obtained in the RPA approximation is,

$$V_{eff} = \sum_{ij,\mathbf{k},\mathbf{k}'} \Gamma_{ij}(\mathbf{k}, \mathbf{k}') c_{i\mathbf{k}\uparrow}^\dagger c_{i-\mathbf{k}\downarrow}^\dagger c_{j-\mathbf{k}'\downarrow} c_{j\mathbf{k}'\uparrow} \quad (3)$$

where the momenta \mathbf{k} and \mathbf{k}' are restricted to different FS C_i with $\mathbf{k} \in C_i$ and $\mathbf{k}' \in C_j$ and $\Gamma_{ij}(\mathbf{k}, \mathbf{k}')$ is the pairing scattering vertex in the singlet channel[26]. The pairing vertex is,

$$\Gamma_{ij}(\mathbf{k}, \mathbf{k}') = Re \left[\sum_{l_1 l_2 l_3 l_4} a_{v_i}^{l_2,*}(\mathbf{k}) a_{v_i}^{l_3,*}(-\mathbf{k}) \times \Gamma_{l_1 l_2 l_3 l_4}(\mathbf{k}, \mathbf{k}', \omega=0) a_{v_j}^{l_1}(\mathbf{k}') a_{v_j}^{l_4}(-\mathbf{k}') \right], \quad (4)$$

where a_v^l (orbital index l and band index v) is the component of the eigenvectors from the diagonalization of the tight binding Hamiltonian. The orbital vertex function $\Gamma_{l_1 l_2 l_3 l_4}$ in the fluctuation exchange formulation[26–28] are given by,

$$\Gamma_{l_1 l_2 l_3 l_4}(\mathbf{k}, \mathbf{k}', \omega) = \left[\frac{3}{2} \bar{U}^s \chi_1^{RPA}(\mathbf{k} - \mathbf{k}', \omega) \bar{U}^s + \frac{1}{2} \bar{U}^s - \frac{1}{2} \bar{U}^c \chi_0^{RPA}(\mathbf{k} - \mathbf{k}', \omega) \bar{U}^c + \frac{1}{2} \bar{U}^c \right]_{l_3 l_4 l_1 l_2}. \quad (5)$$

The \bar{U}^s is the spin interaction matrix and the \bar{U}^c the charge spin interaction matrix, defined in Ref.[26]. The χ_0^{RPA} describes the charge fluctuation contribution and the χ_1^{RPA} the spin fluctuation contribution. For a given gap function $g(\mathbf{k})$, the pairing strength functional is,

$$\lambda[g(\mathbf{k})] = - \frac{\sum_{ij} \oint_{C_i} \frac{dk_{\parallel}}{v_F(\mathbf{k})} \oint_{C_j} \frac{dk'_{\parallel}}{v_F(\mathbf{k}')} g(\mathbf{k}) \Gamma_{ij}(\mathbf{k}, \mathbf{k}') g(\mathbf{k}')}{4\pi^2 \sum_i \oint_{C_i} \frac{dk_{\parallel}}{v_F(\mathbf{k})} [g(\mathbf{k})]^2}, \quad (6)$$

where $v_F(\mathbf{k}) = |\nabla_{\mathbf{k}} E_i(\mathbf{k})|$ is the Fermi velocity on a given fermi surface sheet C_i . $g(\mathbf{k})$ is determined as the station solution of Eq. 6. The obtained gap function should have the symmetry of one of the irreducible representations of the corresponding point group. Although the point group for the BiS_2 layer is C_{4v} , the point group symmetry in our effective model is D_{4h} . We consider one dimensional irreducible representations A_{1g} , A_{2g} , B_{1g} and B_{2g} . We perform calculations in the spin-rotational invariance case, where $U' = U - 2J$ and $J = J'$. The typical temperature $T = 0.02$ is used and $\eta = 0.005$ is adopted to regularize the Green's functions. All the summations over the Brillouin Zone are performed with uniform 200×200 meshes.

First, we consider the case where the Hund's rule coupling is negligible compared with the intraorbital Coulomb interaction. Fig. 2(a) shows the pairing strength eigenvalues for the

four leading eigenvalues as a function of U at the electron doping $x=0.14$. We find that the dominant gap function has the symmetry A_{2g} and the order parameter of this state is shown in Fig.2(b) for $U = 2.5$. This pairing symmetry is g -wave, which changes sign 8 times in a 2π rotation. This state is odd over all the mirror reflections(x,y and diagonal reflections). Therefore, nodes appear in the $k_x/y = 0, \pi$ lines. There is also a sign change within FS sheets. Fig.2(c) shows the subdominant gap function which has A_{1g} symmetry. This extended s -wave state features a sign change and an anisotropic gap distribution on the FS sheets. We can calculate the contributions of intra-sheet and inter-sheet scattering processes for the two leading pairing states separately. We find that the intra-sheet process contributes negatively to the g -wave state while inter-sheet process contributes positively. Both of them show rapid increase with the increasing of U . As the inter-sheet scattering always overcomes the intra-sheet scattering, the A_{2g} is stable. The contribution of both intra-sheet and inter-sheet processes are positive for the A_{1g} s -wave. The strong inter-pocket nesting results in a sign change of the superconducting order between the green p_X (red p_Y) regions on the two electron pockets shown in Fig.1(c). This is the essential reason why the g -wave symmetry is more stable than the s -wave with the increasing of U .

Second, we consider the effect of Hund's coupling on the pairing symmetry. Fig.2(d) shows the pairing strength λ for the four leading eigenvalues as a function of J with $U = 2.5$ and $x = 0.14$. The figure shows that J has a significant effect on the g -wave state but a negligible effect on the s -wave state. Around $J \sim 0.55$, the g -wave pairing and a $B_{1g}(d_{x^2-y^2})$ pairing become equally favored. The d -wave pairing state (not shown) is quite similar to that shown in Fig.3(b). There is no sign change on the same pocket but a sign change between the two pockets. Due to the enhancement of inter orbital scattering with the increasing of J , both intra and inter orbital scattering in the inter-pocket processes become important. Then, the system favors a gap with a sign change between the FS sheets. Consequently, the gap with symmetry $d_{x^2-y^2}$ is favored. However, as shown in Fig.2(d), the pairing strength eigenvalues of the four leading state are very close to each other, indicating the intense competition between those states.

When the electron filling is less than 0.14, we find the g -wave state is always strongly favored if J is relative small. With the increasing of electron doping, the pockets enlarge and the shapes deviate from rectangle. The inter-pocket nesting becomes weaker while the intra-pocket nesting becomes stronger, which greatly affects the pairing strength of the g -wave pairing. In fact, we find that the g -wave and the $d_{x^2-y^2}$ -wave (B_{1g}) are almost equally favored at $x = 0.25$ when $U = 1.75$ and $J = 0.17$. The two leading gap functions are shown in Fig.3. Near the Lifshitz transition point($x=0.45$), the two leading states are the s -wave A_{1g} and the d -wave B_{2g} , shown in Fig.4. The symmetries of the two leading gaps are the same as those at higher electron doping(after Lifshitz transition), studied in Ref.[21]. Nevertheless, there are always strong competitions among multi-pairing channels at

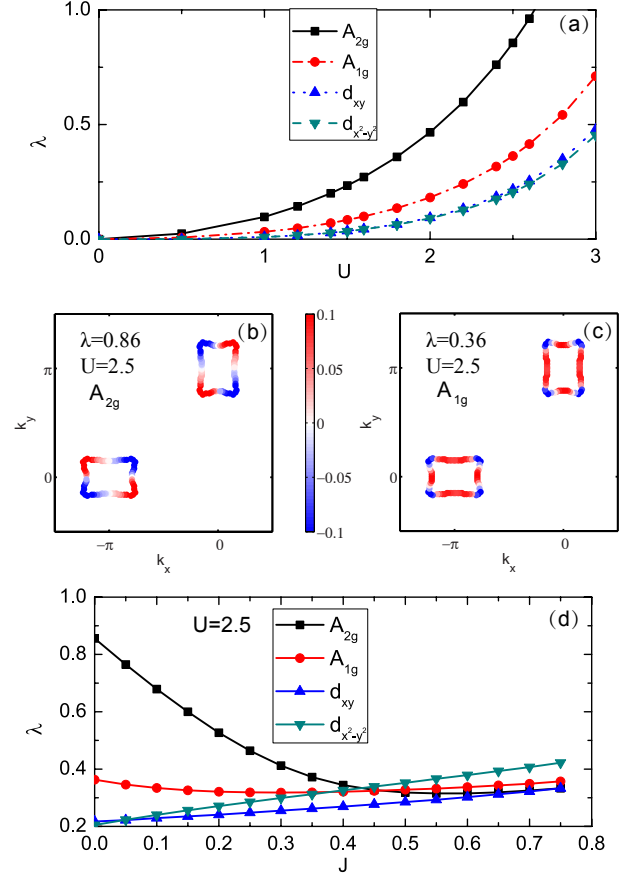


FIG. 2: (Color online) The pairing strengths λ and gap functions for the electron doped compound($x=0.14$) for $J = 0$. (a) The four largest pairing strengths as a function of U . The two dominant gap functions for A_{2g} (b) and A_{1g} (c), calculated close to the instability ($U=2.5$). (d) The four largest pairing strengths as a function of J with $U=2.5$.

high electron doping. There is no obviously leading pairing symmetry.

We use FRG calculations to justify the above RPA results. The FRG approach is described in Ref.[29, 30]. Each electron pocket is discretized into 128 patches. With $U=2.5$ and $J=0.25$, we find a very weak pairing divergence for electron doped system($x=0.14$), shown in Fig.5. Although there is no instability in FRG flow, the calculation can still tell us that g -wave A_{2g} state is more likely to be developed than s -wave A_{1g} state, which is consistent with the results of RPA. The pairing form factors of the two channels are shown in Fig.6(a) and (b), which are quite similar to the corresponding gaps obtained from RPA. The FRG result shows that the pairing strength of the g -wave state become weaker with the increasing of J but it is always the leading one for $J < 0.5$. We also perform calculation with larger U and find that the g -wave state is always the leading one if $J/U < 0.2$. When $J/U > 0.2$, the leading pairing symmetry becomes the $d_{x^2-y^2}$ -wave (B_{1g} state). The g -wave state is robust in a wide range of electron doping

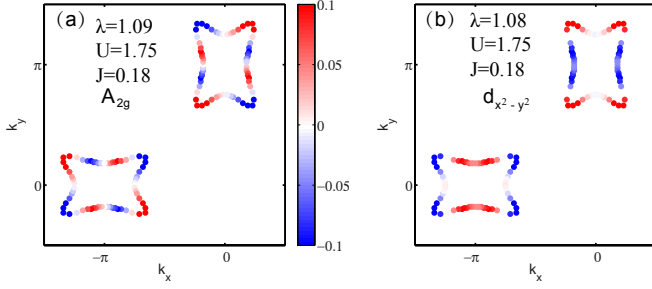


FIG. 3: (Color online) The two dominant gap functions with symmetries A_{2g} (a) and B_{1g} (b) at $x=0.25$, calculated with $U = 1.75$ and $J = 0.18$. The two pairing states are almost degenerate.

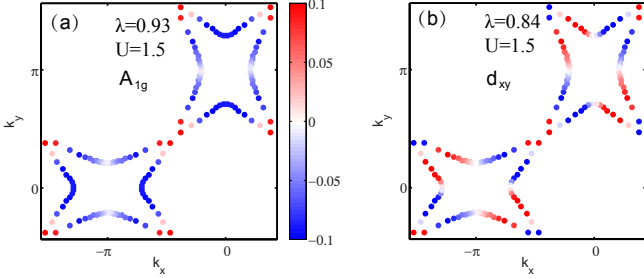


FIG. 4: (Color online) The two dominant gap functions with symmetries A_{1g} (a) and B_{2g} (b) at $x=0.45$, calculated with $U = 1.5$ and $J = 0$.

before the Lifshitz transition if J is relative small. However, the leading pairing symmetry becomes the s-wave A_{1g} close to the Lifshitz transition point. The subleading pairing symmetry is the $d_{x^2-y^2}$ -wave, which slightly differs from the one obtained by RPA calculations.

As the Hund's coupling is relatively weak, the g-wave is robustly favored for BiS_2 superconductors at low doping. The superconducting gap is quite similar to that of g-wave state proposed for cuprate[31]. In fact, the low doping region is the only region that a single g-wave pairing can stand out. If one checks the pairing symmetry near Lifshitz transitions, all results show that no pairing symmetry is clearly favored[21]. At high doping region, two degenerate A_{1g} and B_{2g} states compete with each other in the RPA calculation. While, a similar A_{1g} state is obtained but no competing B_{2g} state in Ref.[20], where the strong coupling t-J model is adopted. This indicates B_{2g} state is suppressed with the increasing of interaction. As our calculations mainly focus on the experimental low doping levels, the pairing symmetry is different from the previous studies that focus on relative high doping levels[12, 21, 22]. Actually, near the Lifshitz transition point, the obtained pairing symmetry is consistent with that of Ref.[21].

In the above calculation, we do not consider spin orbital coupling in Bi. Due to the absence of p_z orbitals, the spin orbital coupling does not involve spin-flips and spin is still a good quantum number. The spin orbital coupling has little effect on the topology of FSs and the distribution of orbital

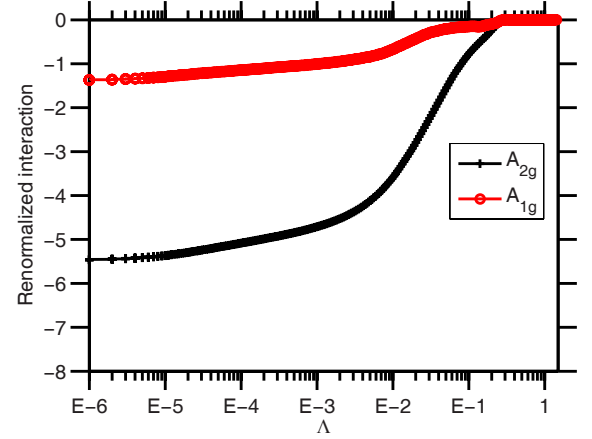


FIG. 5: (Color online) FRG flow of two leading pairing channels for the electron doped compound($x=0.14$) with $U=2.5$ and $J=0.25$.

characters on FSs. Therefore, we should expect that spin orbital coupling has little effect on the pairing symmetry in BiS_2 superconductors.

Can we find other materials with g-wave pairing symmetry? Like the high T_c materials, we consider materials containing d orbitals. The correlation effect in d orbitals is much stronger than that of p orbital. We consider a material where the states near the Fermi level are mainly contributed by d_{xz} and d_{yz} orbitals due to the crystal field splitting. The Fermi surfaces and orbital characters($d_{xz} \sim p_x$, $d_{yz} \sim p_y$) are similar to those in Fig.1(c), where electron or hole pockets are around X point. If this system becomes superconducting, the pairing symmetry may be g-wave. This can help us to find g-wave superconducting materials.

The g-wave pairing state can be easily justified or falsified by experiments. The most distinct feature is the symmetry protected nodes on Fermi surfaces as shown Fig.2(b). There are 8 nodal points on Fermi Surfaces. The high resolution ARPES can directly probe the nodal structure. Physical properties related to low energy excitations, such as thermal conductivity, spin relaxation and penetration depth, should be very similar to the d-wave state in cuprates.

In summary, we have studied the pairing properties of BiS_2 based superconductors at low electron doping level using RPA and FRG methods. Our calculations suggest that a g-wave(A_{2g}) state is dominant at electron doping $x < 0.25$ when Hund's rule coupling is relative small compared with intra-orbital Coulomb interactions($J \leq 0.2U$). The g-wave state can be falsified by its distinctive nodal structures. A proof of the g-wave will not only crown BiS_2 as the first superconductor with the g-wave pairing, but also shed light on the mechanism of unconventional superconductors.

The work is supported by "973" program (Grant No. 2010CB922904 and No. 2012CV821400), as well as national science foundation of China (Grant No. NSFC-1190024, 11175248 and 11104339).

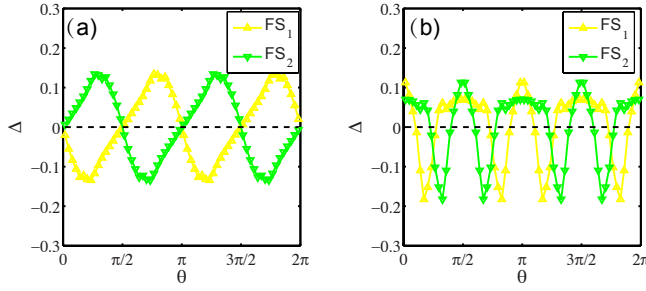


FIG. 6: (Color online) Gap form factors for the two leading pairing channels for the electron doped compound ($x=0.14$) with $U=2.5$ and $J=0.25$ in FRG calculations. (a) The leading A_{2g} gap. (b) The sub-leading A_{1g} gap. θ is the polar angle on each FS with respect to its center and $\theta = 0$ indicates the $+k_x$ direction. The yellow (upward triangles) and green (downward triangles) lines label the two electron FS centered at $(\pi, 0)$ and $(0, \pi)$, respectively.

* Electronic address: jphu@iphy.ac.cn

- [1] Y. Mizuguchi, H. Fujihisa, Y. Gotoh, K. Suzuki, H. Usui, K. Kuroki, S. Demura, Y. Takano, H. Izawa and O. Miura, Phys. Rev. B **86**, 220510 (2012).
- [2] S. K. Singh, A. K., B. Gahtori, G. Sharma, S. Patnaik, and V. P. S. Awana, J. Am. Chem. Soc. **134** 16504(2012).
- [3] Y. Mizuguchi, S. Demura, K. Deguchi, Y. Takano, H. Fujihisa, Y. Gotoh, H. Izawa, and O. Miura, J. Phys. Soc. Jpn. **81**, 114725 (2012).
- [4] S. Demura, Y. Mizuguchi, K. Deguchi, H. Okazaki, H. Hara, T. Watanabe, S. Denholme, M. Fujioka, T. Ozaki, H. Fujihisa, Y. Gotoh, O. Miura, T. Yamaguchi, H. Takeya, Y. Takano, J. Phys. Soc. Jpn., **82**, 033708 (2013).
- [5] J. Xing, S. Li, X. Ding, H. Yang, and H.-H. Wen, Phys. Rev. B **86**, 214518 (2012).
- [6] R. Jha, S. Singh, and V. P. S. Awana, J. Supercond. Novel Magn. **26**, 499 (2013).
- [7] X. Lin, X. X. Ni, B. Chen, X. F. Xu, X. X. Yang, J. H. Dai, Y. K. Li, X. J. Yang, Y. K. Luo, Q. Tao, G. H. Cao, and Z. A. Xu, Phys. Rev. B **87**, 020504(R) (2013).
- [8] D. Yazici, K. Huang, B. D. White, I. Jeon, V. W. Burnett, A. J. Friedman, I. K. Lum, M. Nallaiyan, S. Spagna, and M. B. Maple, Phys. Rev. B **87**, 174512 (2013).
- [9] K. Deguchi, Y. Mizuguchi, S. Demura, H. Hara, T. Watanabe, S. J. Denholme, M. Fujioka, H. Okazaki, T. Ozaki, H. Takeya, T. Yamaguchi, O. Miura, and Y. Takano, Europhys. Lett. **101**, 17004 (2013).
- [10] P. K. Biswas, A. Amato, C. Baines, R. Khasanov, H. Luetkens, Hechang Lei, C. Petrovic, E. Morenzoni, arxiv:1309.7282 (2013).
- [11] Y. K. Li, X. Lin, L. Li, N. Zhou, X. F. Xu, C. Cao, J. H. Dai, L. Zhang, Y. K. Luo, W. H. Jiao, Q. Tao, G. H. Cao, Z. Xu, Supercond. Sci. Technol. **27**, 035009 (2014).
- [12] H. Usui, K. Suzuki and K. Kuroki. Phys. Rev. B **86**, 220501 (2012).
- [13] X. G. Wan, H. C. Ding, Sergey Y. Savrasov and C. G. Duan, Phys. Rev. B **87**, 115124 (2013).
- [14] B. Li, Z. W. Xing and G. Q. Huang. Europhys. Lett. **101**, 47002 (2013).
- [15] T. Yildirim, Phys. Rev. B **87**, 020506(R) (2013).
- [16] J. Lee, M. B. Stone, A. Huq, T. Yildirim, G. Ehlers, Y. Mizuguchi, O. Miura, Y. Takano, K. Deguchi, S. Demura, and S.-H. Lee, Phys. Rev. B **87**, 205134 (2013).
- [17] S. Li, H. Yang, D. Fang, Z. Wang, J. Tao, X. Ding, and H. H. Wen, Sci. China-Phys. Mech. Astron. **56**, 2019 (2013).
- [18] J. Z. Liu, D. L. Fang, Z. Y. Wang, J. Xing, Z. Y. Du, X. Y. Zhu, H. Yang, and H. H. Wen, arXiv:1310.0377.
- [19] T. Zhou and Z. D. Wang, J. Supercond. Novel Magn. **26**, 2735(2013).
- [20] Y. Liang, X. X. Wu, W. F. Tsai and J. P. Hu. Front. Phys. **9** 194(2014).
- [21] G. B. Martins, A. Moreo, and E. Dagotto, Phys. Rev. B **87**, 081102(R) (2013).
- [22] Y. Yang, W. S. Wang, Y. Y. Xiang, Z. Z. Li, and Q. H. Wang, Phys. Rev. B **88**, 094519 (2013).
- [23] L. K. Zeng, X. B. Wang, J. Ma, P. Richard, S. M. Nie, H. M. Weng, N. L. Wang, Z. Wang, T. Qian, and H. Ding. arxiv:1402.1833.
- [24] Z. R. Ye, H. F. Yang, D. W. Shen, C. J. Jiang, X. H. Niu, D. L. Feng, Y. P. Du, X. G. Wan, J. Z. Liu, X. Y. Zhu, H. H. Wen, and M. H. Jiang. Arxiv:1402.2860.
- [25] S. Graser, T. A. Maier, P. J. Hirschfeld and D. J. Scalapino, New J. Phys. **11** 025016(2009).
- [26] A. F. Kemper, T. A. Maier, S. Graser, H. P. Cheng, P. J. Hirschfeld and D. J. Scalapino, New J. Phys. **12** 073030(2010).
- [27] N. E. Bickers, D. J. Scalapino and S. R. White, Phys. Rev. Lett. **62** 961(1989).
- [28] K. Kubo, Phys. Rev. B **75** 224509 (2007).
- [29] F. Wang, H. Zhai, Y. Ran, A. Vishwanath, and D. H. Lee, Phys. Rev. Lett., **102**, 047005(2009).
- [30] H. Zhai, F. Wang and D. H. Lee, Phys. Rev. B, **80** 064517(2009).
- [31] P. V. Shevchenko, and O. P. Sushkov, Physica C, **295**, 292(1998).